

SuperSuit: An Isomorphic Bimodal Interface for Scalable Mobile Manipulation

Tongqing Chen^{1,2}, Hang Wu², Jiasen Wang², Xiaotao Li², Zhu Jin², Lu Fang^{1,†}

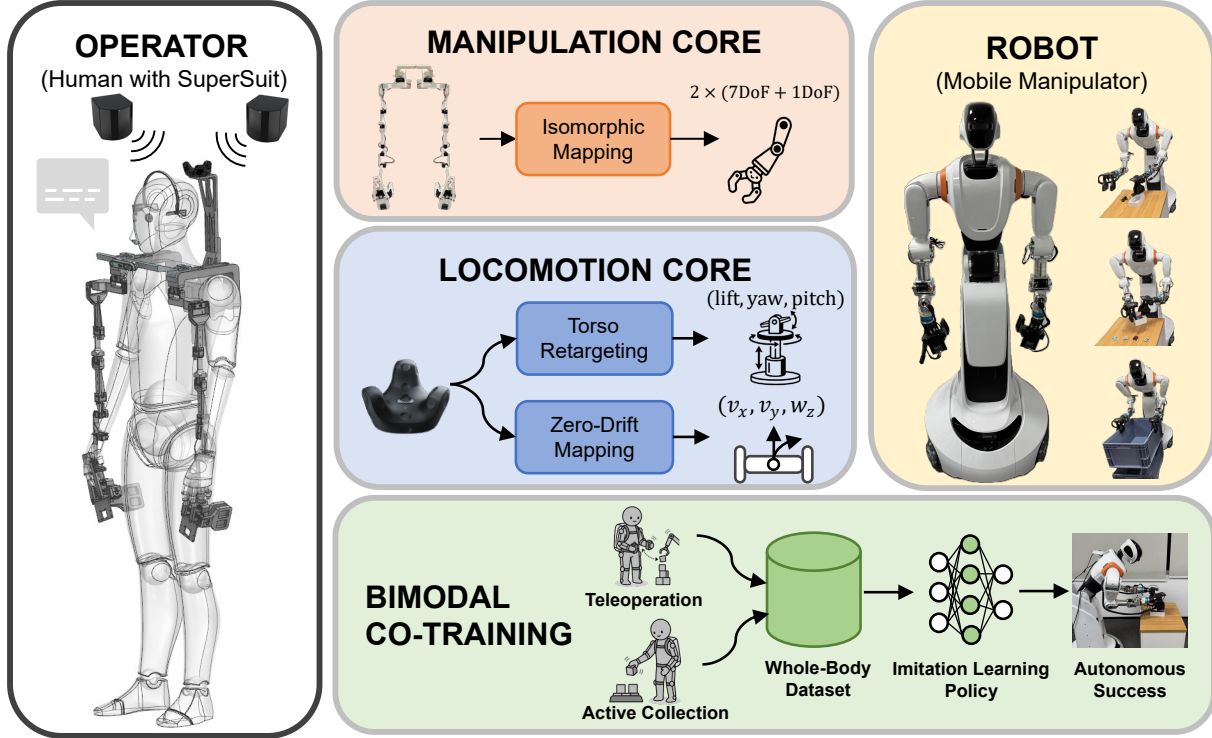


Fig. 1: **The SuperSuit Framework.** Our untethered wearable interface translates human embodiment into whole-body robot control via strict isomorphic arm manipulation and zero-drift base locomotion. This synergistic architecture natively supports bimodal data acquisition (teleoperation and active collection), generating high-fidelity datasets that directly fuel imitation learning policies for autonomous mobile manipulation.

Abstract—High-quality, long-horizon demonstrations are essential for embodied AI, yet acquiring such data for tightly coupled wheeled mobile manipulators remains a fundamental bottleneck. Unlike fixed-base systems, mobile manipulators require continuous coordination between $SE(2)$ locomotion and precise manipulation, exposing limitations in existing teleoperation and wearable interfaces. We present SuperSuit, a bimodal data acquisition framework that supports both robot-in-the-loop teleoperation and active demonstration under a shared kinematic interface. Both modalities produce structurally identical joint-space trajectories, enabling direct data mixing without modifying downstream policies. For locomotion, SuperSuit maps natural human stepping to continuous planar base velocities, eliminating discrete command switches. For manipulation, it employs a strictly isomorphic wearable arm in both modes, while policy training is formulated in a shift-invariant delta-joint representation to mitigate calibration

offsets and structural compliance without inverse kinematics. Real-world experiments on long-horizon mobile manipulation tasks show $2.6\times$ higher demonstration throughput in active mode compared to a teleoperation baseline, comparable policy performance when substituting teleoperation data with active demonstrations at fixed dataset size, and monotonic performance improvement as active data volume increases. These results indicate that consistent kinematic representations across collection modalities enable scalable data acquisition for long-horizon mobile manipulation.

I. INTRODUCTION

Despite the success of imitation learning in short-horizon skills [1]–[8], the advancement of embodied AI toward complex, long-horizon tasks remains fundamentally bottlenecked by the lack of high-quality demonstration data [9]–[11]. Wheeled mobile manipulators [12], [13], which integrate the expansive $SE(2)$ workspace of a mobile base with the dexterity of robotic arms, represent an ideal hardware morphology for unstructured household environments. However, acquiring high-fidelity, whole-body demonstrations for these

[†]Corresponding author.

¹Tongqing Chen and Lu Fang are with Tsinghua University, Beijing, China. Email: ctq24@mails.tsinghua.edu.cn, fanglu@tsinghua.edu.cn. ²Hang Wu, Jiasen Wang, Xiaotao Li and Zhu Jin are with TARS Robotics, Shanghai, China. Email: {wuhang, wangjiasen, lixiaotao, albert}@tars-ai.com.

coupled systems remains a formidable challenge due to the severe limitations of existing teleoperation interfaces.

Current teleoperation paradigms, such as BRS [14] and HOMIE [15], suffer from profound cognitive and perceptual decoupling. Relying on joysticks or pedals while observing through occluded, 2D camera streams fractures the operator’s sense of embodiment and degrades the intuitive spatial awareness required for fine-grained tasks. Furthermore, these remote “cockpit” systems impose a scalability bottleneck: the rigid 1:1 human-robot coupling tethers human expertise to active hardware uptime, making large-scale data acquisition prohibitively slow and costly.

To capture walking intent, frameworks like HumanoidExo [16] and EgoHumanoid [17] pair wearable exoskeletons with LiDAR-SLAM [18] or spatial trackers. While effective for bipedal navigation, these systems typically achieve intent-level alignment, where complex controllers translate human gait into robot-specific motion. In contrast, wheeled robots permit a natural alignment with high-level decision spaces through direct velocity mapping. Moreover, accumulated SLAM drift can fatally misalign manipulation trajectories in precision-sensitive tasks, yielding suboptimal data for imitation learning.

For arm manipulation, prevalent interfaces (e.g., UMI [19], DexUMI [20], and HuMI [21]) rely on 6D task-space tracking with Inverse Kinematics (IK), which is prone to singularities, non-unique solutions, and kinematically unreachable targets. To avoid IK, some systems employ direct joint correspondence; however, naive absolute joint control is sensitive to calibration offsets, gear backlash, and structural compliance, leading to systematic trajectory deviations between demonstration and execution.

To address these limitations, we introduce **SuperSuit**, a unified bimodal wearable framework for whole-body data acquisition in mobile manipulation. By preserving a shared kinematic interface, SuperSuit supports both active demonstration and direct robot-in-the-loop teleoperation. Crucially, the system features an integrated headset microphone to capture in-situ verbal narrations during demonstrations. This continuous audio stream naturally segments and semantically aligns physical trajectories with corresponding language instructions, providing high-fidelity subtask supervision for downstream Vision-Language-Action (VLA) models.

For locomotion, head-mounted spatial tracking drives a torso-referenced kinematic decomposition that maps human motion to torso articulation and continuous base velocities, while a velocity-level decoupling mechanism suppresses involuntary micro-sway. For manipulation, a strictly isomorphic wearable arm formulates control and data logging via joint-space delta increments (Δq_i). This shift-invariant representation mitigates calibration offsets and ensures structural consistency across both modalities, natively unifying the dataset for downstream policy learning.

In summary, our main contributions are as follows:

- We present **SuperSuit**, a bimodal isomorphic wearable framework that unifies active human demonstration and robot-in-the-loop teleoperation under a shared whole-

body kinematic interface, enabling structurally consistent data collection across modalities.

- We introduce robust whole-body retargeting, combining continuous stepping-to-velocity locomotion with a shift-invariant delta-joint manipulation formulation to eradicate calibration errors and structural compliance.
- We integrate an in-situ verbal narration mechanism into the whole-body collection framework, utilizing continuous audio streams to automatically extract structurally aligned, language-conditioned subtasks for downstream VLA policies.
- Through extensive real-world experiments on long-horizon mobile manipulation tasks, we demonstrate $2.6\times$ higher data collection throughput, comparable policy performance when substituting teleoperation data with active demonstrations, and consistent performance gains as active data volume increases.

II. RELATED WORK

A. Robot-in-the-Loop Teleoperation for Data Collection

Robot-in-the-loop teleoperation is widely used for whole-body data collection on humanoid and wheeled mobile platforms. For humanoids, recent systems employ immersive interfaces and full-body retargeting under balance constraints [22]–[28], requiring real-time stabilization of high-DoF dynamics during demonstration. For wheeled mobile manipulators, locomotion and manipulation are typically decoupled: platforms such as Mobile ALOHA [13] and BRS [14] use bimanual interfaces for arm control while base motion is mediated through joysticks or auxiliary channels. This separation disrupts natural whole-body coordination during data collection.

Across both paradigms, teleoperation binds data acquisition to real-time hardware execution. Demonstrations must satisfy platform constraints during recording, and throughput remains limited by robot availability and safety considerations, restricting scalability.

B. Robot-Free and Embodied Demonstration Interfaces

Robot-free data collection has enabled scalable manipulation learning on fixed-base manipulators [19], [20], [29]–[32]. These approaches typically focus on manipulation without explicitly modeling locomotion–manipulation coupling. Recent extensions to mobile or humanoid platforms [21], [33]–[35] primarily capture 6D end-effector motion and rely on IK or reinforcement learning (RL), which introduce kinematic infeasibility and limited final positioning accuracy in high-DoF whole-body systems.

Isomorphic exoskeleton interfaces [36]–[38] avoid IK through joint-space alignment but are largely limited to upper-limb control in fixed-base settings. In contrast, SuperSuit provides a strictly isomorphic joint-space interface spanning both arm manipulation and mobile base control, enabling whole-body robot-free data collection for mobile manipulation.

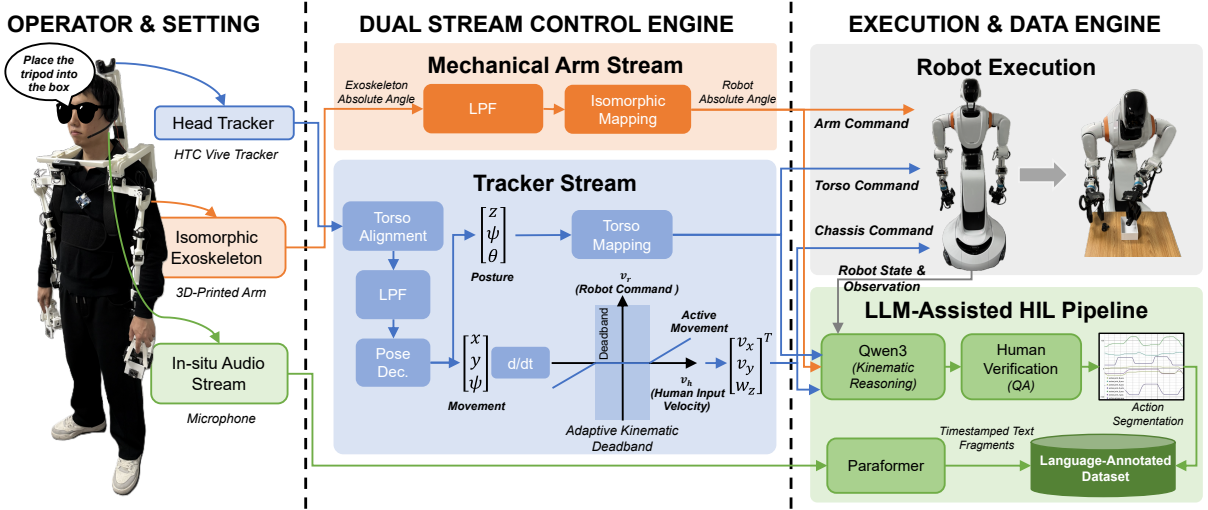


Fig. 2: **System Architecture of SuperSuit.** Multimodal human intent is captured and decoupled via a Dual Stream Control Engine. The Dual Stream Control Engine decouples human motion into: (1) Mechanical Arm Stream for upper-body isomorphic mapping, and (2) Tracker Stream for torso and base control. Specifically, the tracker-based 6D pose is decomposed into articulated torso configurations and planar locomotion velocities. A velocity-level deadband is applied to suppress involuntary micro-sway. These robust signals simultaneously drive the mobile manipulator and feed into an LLM-assisted HIL pipeline, merging Qwen3 kinematic reasoning with Paraformer transcriptions to automatically generate high-fidelity, language-annotated datasets for VLA models.

III. METHODOLOGY

A. System Overview

The SuperSuit system, as comprehensively illustrated in Fig. 2, is designed as an end-to-end, bimodal data collection and teleoperation infrastructure for wheeled mobile manipulators. Hardware-wise, the operator’s upper body is equipped with a lightweight, 3D-printed isomorphic exoskeleton that structurally mirrors the kinematics of the target robotic arm. Simultaneously, the operator’s global locomotion intent is reliably captured via a single head-mounted HTC Vive Tracker, localized by HTC Base Station 2.0 lighthouses to ensure sub-millimeter spatial accuracy while explicitly eliminating bimanual signal occlusion. Furthermore, an integrated headset microphone allows the operator to verbally narrate subtask descriptions in real-time during the demonstration. Software-wise, our unified control pipeline seamlessly processes these disparate sensory and audio inputs to generate continuous, singularity-free commands for the robot’s whole-body execution.

Crucially, the system supports two distinct data collection modalities: *Remote Teleoperation* and *Active Demonstration*, as illustrated in Fig. 3 and Fig. 4, respectively. Both modalities share the identical shift-invariant data formulation and automated language annotation pipeline, ensuring that all collected demonstrations are inherently standardized for downstream policy learning.

B. Human-to-Torso-and-Base Kinematic Retargeting

To avoid severe signal occlusion during bimanual manipulation, the spatial tracker is mounted on the operator’s head. However, the robot control reference is defined at the

articulated torso (specifically the torso pitch link) and the mobile base. We therefore perform an offline rigid calibration to align the head-mounted tracker frame with the robot torso reference frame.

Let the tracker pose in the world frame be $\mathbf{T}_h(t)$, and let \mathbf{T}_{cal} denote the fixed transformation from the tracker frame to the torso pitch link frame. To mitigate sensor noise and small-amplitude tracking fluctuations, the raw pose stream is temporally smoothed using a low-pass filter before calibration and motion decomposition. The torso-referenced human pose is computed as

$$\mathbf{T}_{torso}^h(t) = \mathbf{T}_{cal} \mathbf{T}_h(t). \quad (1)$$

We decompose this pose into translation and orientation components:

$$\mathbf{T}_{torso}^h(t) \Rightarrow (x(t), y(t), z(t), \psi(t), \theta(t), \phi(t)),$$

where (x, y, z) denote the torso-frame position and ψ, θ, ϕ correspond to yaw, pitch, and roll, respectively.

The torso lift, yaw, and pitch joints are directly obtained from the vertical displacement and orientation components (z, ψ, θ) , forming the articulated torso configuration $\mathbf{q}_{torso}(t)$.

The planar locomotion component is obtained by projecting the torso-referenced pose onto the ground plane:

$$\mathbf{p}(t) = \begin{bmatrix} x(t) \\ y(t) \\ \psi_{base}(t) \end{bmatrix}.$$

Planar velocities are computed via discrete differentiation:

$$\dot{x}(t) \approx \frac{x(t) - x(t - \Delta t)}{\Delta t}, \quad \dot{y}(t) \approx \frac{y(t) - y(t - \Delta t)}{\Delta t}, \quad (2)$$

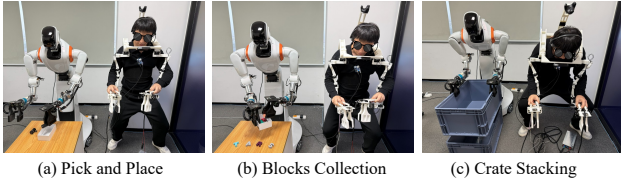


Fig. 3: **Remote Teleoperation Mode.** SuperSuit enables intuitive, zero-latency bimanual manipulation across diverse spatial tasks: (a) Pick and Place, (b) Blocks Collection, and (c) Crate Stacking.

$$\omega_z(t) \approx \frac{\text{wrap}(\psi_{\text{base}}(t) - \psi_{\text{base}}(t - \Delta t))}{\Delta t}. \quad (3)$$

Assuming alignment between the planar reference frame and the base link, the commanded base velocity is $(v_x, v_y, \omega_z) = (\dot{x}, \dot{y}, \dot{\omega}_z)$, whose integration drives the mobile platform to follow the human planar pose.

Depending on task requirements, the human yaw motion can be assigned either to the mobile base for global reorientation or to the torso joint for local manipulation alignment.

Despite temporal smoothing, differentiated human motion still contains small involuntary micro-sway induced by natural posture stabilization. If directly integrated into base commands, these micro-motions lead to undesirable base jitter during contact-rich manipulation.

To suppress unintended oscillations we employ an adaptive kinematic deadband at the velocity level. Let $v_{h,x}(t), v_{h,y}(t), \omega_h(t)$ denote the planar velocities derived from the filtered torso-referenced pose. A dimensional deadband operator $\mathcal{D}(v, \epsilon)$ is applied such that velocities within a small threshold are suppressed, while deliberate motions pass through unchanged.

The resulting base command is given by

$$\begin{bmatrix} v_x(t) \\ v_y(t) \\ \omega_z(t) \end{bmatrix} = \begin{bmatrix} K_x \mathcal{D}(v_{h,x}(t), \epsilon_x) \\ K_y \mathcal{D}(v_{h,y}(t), \epsilon_y) \\ K_\omega \mathcal{D}(\omega_h(t), \epsilon_\omega) \end{bmatrix}. \quad (4)$$

This continuous decoupling mechanism preserves intentional locomotion while eliminating posture-induced jitter, enabling seamless transitions between navigation and precision manipulation.

C. Strict Isomorphism and Robust Action Formulation

While isomorphic systems bypass Inverse Kinematics (IK), their reliance on absolute joint mapping remains vulnerable to gear backlash, structural compliance, and human-to-exoskeleton calibration offsets. These uncompensated errors propagate through the kinematic chain, resulting in significant cumulative inaccuracies during physical deployment. To mitigate these effects, the SuperSuit is engineered with strict kinematic isomorphism, as illustrated in Fig. 5. By explicitly aligning its mechanical rotational axes with the operator’s anatomical degrees of freedom, this structural mirroring establishes a bijective mapping for direct joint-space control, bypassing Cartesian transformations entirely. Furthermore, to ensure kinematic stability against high-frequency noise,

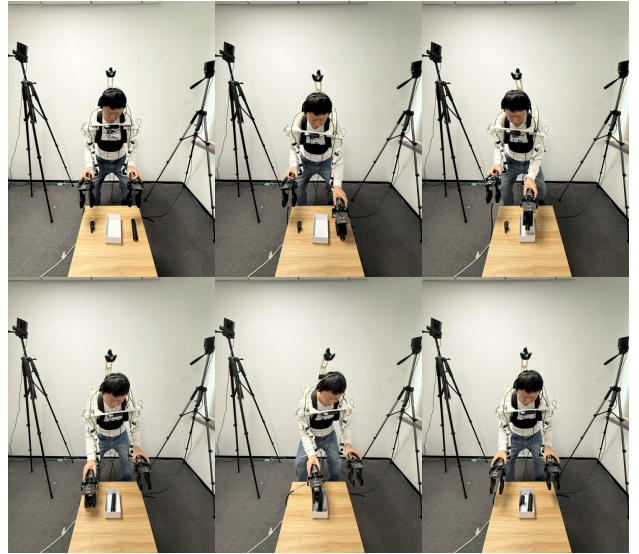


Fig. 4: **Active Demonstration Mode.** A continuous sequence of the Pick and Place benchmark performed directly by the operator.

the raw joint sequences are processed via LPF to yield the smoothed human intent \mathbf{q}_t .

While the system records absolute joint positions from the exoskeleton, relying purely on absolute poses makes the policy susceptible to static calibration offsets. To address this, the arm action \mathbf{a}_t utilized for policy training and inference is formulated as a relative, forward-looking positional increment. Formally, given the current joint state \mathbf{q}_t , the action represents the positional delta required to reach a target configuration at a future timestep:

$$\mathbf{a}_t = \Delta \mathbf{q}_t = \mathbf{q}_{t+k} - \mathbf{q}_t \quad (5)$$

where k denotes the look-ahead horizon (e.g., the terminal point of an action chunk).

This forward-looking formulation is crucial for enhancing the robustness of the learned policy. While historical joint differences $(\mathbf{q}_t - \mathbf{q}_{t-1})$ are implicitly encoded as joint velocities within the observation state s_t to provide temporal context, the action \mathbf{a}_t explicitly dictates the transition to the robot’s next target setpoint $(\mathbf{q}_t + \mathbf{a}_t \rightarrow \mathbf{q}_{t+k})$.

By adopting this shift-invariant $\Delta \mathbf{q}$ action space, the system effectively mitigates static calibration errors, as any constant physical offset is canceled out during the differencing operation. Concurrently, the temporal filtering applied prior to this step ensures a smooth action trajectory suitable for high-frequency, closed-loop control.

D. LLM-Assisted Human-in-the-Loop Annotation Pipeline

The ultimate objective of the SuperSuit architecture is to scale the acquisition of high-fidelity, language-conditioned data for modern embodied AI policies. During data collection, the system synchronously logs the robot’s multi-modal observations and the continuous action vector $\mathbf{a}_t = [\Delta \mathbf{q}_t, v_x(t), \omega_z(t), \text{gripper}_t]$, alongside a continuous audio

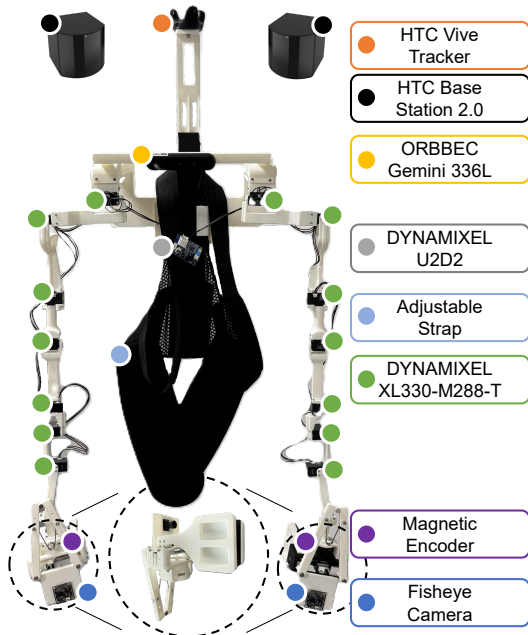


Fig. 5: **Kinematic Alignment of the SuperSuit.** The exoskeleton’s mechanical axes structurally mirror the operator’s anatomical degrees of freedom. (Note: The grippers are 3D printed in white for visual clarity and teleoperation, whereas actual data collection employs black grippers identical to the target robot’s configuration.)

stream of the operator’s in-situ verbal narration. To efficiently generate strictly aligned Visuomotor datasets, we propose a Human-in-the-Loop (HIL) dual-stream annotation architecture. First, the raw audio is transcribed into timestamped text strings using Paraformer [39], a highly efficient non-autoregressive Speech-to-Text model. Because human speech inherently suffers from temporal misalignment relative to physical execution, we employ Qwen3 [40] as an initial kinematic reasoning engine. Qwen3 analyzes the underlying action sequences to propose physical breakpoints (e.g., zero-velocity crossings and gripper state toggles) and temporally maps the Paraformer-transcribed text to these boundaries. To ensure the absolute fidelity required by foundation models, human operators rapidly verify and refine the LLM-proposed boundaries. Ultimately, this HIL pipeline guarantees that each extracted subtask is precisely bounded by physical state transitions and synchronized with its corresponding language instruction \mathcal{L}_t .

IV. EXPERIMENTS

To rigorously evaluate the efficacy of the SuperSuit architecture, we design a comprehensive suite of real-world mobile manipulation tasks. Our experiments aim to answer three fundamental questions:

(1) **Data Collection Efficiency:** Does SuperSuit significantly increase the number of successful demonstrations collected per hour of human effort compared to state-of-the-art teleoperation baselines?

(2) **Policy Performance:** Can the high-fidelity, zero-drift datasets generated by SuperSuit intrinsically boost the success rates and execution stability of imitation learning architectures?

(3) **Scalability:** Does the performance of downstream policies scale monotonically with the volume of SuperSuit-captured data, and can it facilitate the emergence of complex, long-horizon skills through massive data scaling?

A. Experimental Setup and Benchmark Tasks

Hardware Platform. We evaluate the SuperSuit system on a custom 22-DoF wheeled bimanual humanoid platform designed for unstructured indoor environments. The robot’s kinematic configuration consists of: Two 7-DoF robotic arms, each equipped with a 1-DoF parallel gripper (16 DoF total for manipulation). A 3-DoF active torso supporting lift, yaw, and pitch motions (z, ψ, θ). A 3-DoF mobile base providing planar locomotion (v_x, v_y, ω_z). For visual perception, the system utilizes synchronized RGB streams from a chest-mounted ORBBEC Gemini 336L camera (global view) and bilateral wrist-mounted cameras (localized manipulation views). Fig. 6 explicitly depicts these corresponding egocentric and wrist-level camera perspectives captured across both data acquisition modalities.



(a) Remote Teleoperation Mode



(b) Active Demonstration Mode

Fig. 6: **Bimodal Visuomotor Observations.** Synchronized global (chest-mounted) and localized (wrist-mounted) camera views captured during (a) Remote Teleoperation and (b) Active Demonstration. Both modalities preserve structurally consistent, high-fidelity visual state representations for downstream policy learning.

Policy Training. For imitation learning, we adopt the $\pi_{0.5}$ [41] architecture as our primary baseline policy. Furthermore, to rigorously evaluate the efficacy of the dense subtask language annotations generated by our HIL pipeline, we introduce an augmented variant denoted as $\pi_{0.5}^+$. This variant re-implements the base architecture with an auxiliary autoregressive language head, intrinsically forcing the model to predict structural boundaries and semantic instructions during execution. During joint training, the loss weight for this auxiliary subtask prediction is strictly scaled to 0.1 to prevent interference with the primary visuomotor action

generation. Both models are trained with a batch size of 256 for 10,000 steps using the AdamW optimizer with a constant learning rate of 5×10^{-5} . Unless explicitly stated otherwise, the standard $\pi_{0.5}$ architecture serves as the default policy backbone for all subsequent empirical evaluations.

Task 1: Pick-and-Place. The robot navigates from a starting position to a desk to retrieve a tripod and a connector, placing them into a box. This task benchmarks the integration of mobile navigation and high-precision grasping.

Task 2: Blocks Collection. The robot must hold a receptacle in its right hand while dynamically picking up scattered, irregularly shaped blocks from a desk with its left hand and placing them into the receptacle. This long-horizon task evaluates continuous bimanual coordination and sustained execution consistency over multiple manipulation cycles.

Task 3: Crate Stacking. The robot navigates to a desk, performs a bimanual lift of a large crate, and transports it to a target location for precise stacking. This multi-stage long-horizon task benchmarks integrated locomotion and synchronized bimanual control required to maintain stability and alignment across operational phases.

Visual examples of the three manipulation tasks during remote teleoperation are comprehensively illustrated in Fig. 3.

B. Data Collection Efficiency

TABLE I: Data Collection Throughput (*episode/hour*) by Task.

Modality	Pick-and-Place	Blocks	Stacking
BRS [14]	56.8	20.7	11.4
SuperSuit (Teleop)	65.1	24.3	13.2
SuperSuit (Active)	151.4	51.9	32.5

We quantitatively evaluate data acquisition efficiency (successful episodes per hour) across three modalities: a custom-adapted BRS-style baseline, SuperSuit Teleoperation, and SuperSuit Active Demonstration. All operators were trained to proficiency, with average throughputs detailed in Table I. As shown, SuperSuit (Teleop) consistently outperforms BRS by 14% to 17% across all tasks. This baseline gain primarily stems from our continuous locomotion interface; while BRS relies on discrete, button-mediated base commands that introduce intermittent alignment pauses, SuperSuit seamlessly maps natural stepping to continuous planar velocities, eliminating micro-adjustment overhead during frequent locomotion-manipulation transitions.

The efficiency gap widens substantially in Active Demonstration mode, achieving a 2.5–2.9 \times throughput increase over BRS (reaching 151.4, 51.9, and 32.5 episodes/hour for the three tasks, respectively). By removing robot-in-the-loop latency and restoring first-person embodiment, Active mode allows operators to directly leverage natural contact feedback, drastically reducing grasp correction cycles and task-level recovery overhead.

Crucially, tasks like Blocks Collection and Crate Stacking demand continuous dual-arm synchronization, which inherently bottlenecks remote teleoperation due to mediated visual

feedback and sequential control attention. SuperSuit’s Active mode completely bypasses this limitation by preserving innate human inter-arm synergy, enabling fluid, simultaneous bimanual adjustments that maximize demonstration yield in coordination-intensive tasks.

C. Policy Performance and Effective Throughput

TABLE II: Policy success rate on different data compositions.

Training Data Composition	Pick-and-Place	Blocks	Stacking
Teleop 10 / Active 0	10%	0%	0%
Teleop 110 / Active 0	85%	65%	40%
Teleop 10 / Active 100	85%	60%	40%

We evaluate the downstream impact of data composition on the $\pi_{0.5}$ policy over 20 independent trials per task, fixing the total dataset size to 110 episodes. As shown in Table II, while training on only 10 teleoperation episodes fails to generalize, scaling to 110 episodes significantly boosts success rates to 85%, 65%, and 40% across the three tasks. However, acquiring continuous teleoperation data at this scale incurs prohibitive hardware wear and operator overhead. Crucially, replacing 100 Teleoperation demonstrations with 100 Active demonstrations yields nearly identical performance (85%, 60%, and 40%), proving that high-throughput Active data can safely substitute hardware-bound teleoperation. We attribute this zero-degradation substitution directly to our strict kinematic isomorphism and shared Δq formulation, which ensure that both human-only and robot-in-the-loop trajectories remain structurally consistent for downstream learning.

TABLE III: Effective Throughput (success/hour)

Training Data Composition	Pick-and-Place	Blocks	Crate
Teleop 10 / Active 0	4.2	0.0	0.0
Teleop 110 / Active 0	41.9	11.4	3.8
Teleop 10 / Active 100	88.8	23.3	9.5

To jointly evaluate data quality and execution efficiency, we define *Effective Throughput* as the expected number of successful autonomous task completions per hour. As detailed in Table III, substituting 100 teleoperation demonstrations with Active data increases effective throughput from (41.9, 11.4, 3.8) to (88.8, 23.3, 9.5), yielding a systematic 2.0–2.5 \times improvement. Given that policy architecture and inference speed remain identical, this gain intrinsically stems from the superior structural properties of Active demonstrations. Unencumbered by remote latency or mediated control, Active first-person demonstrations produce smoother, temporally consistent motion that translates into shorter autonomous execution horizons and significantly fewer recovery behaviors. Ultimately, SuperSuit not only drastically accelerates data collection but inherently fosters more robust, streamlined continuous execution in downstream VLA models.

TABLE IV: Success rate (%) on Crate Stacking as the number of Active demonstrations increases.

Training Data Composition	Success Rate
Teleop 10 / Active 0	0%
Teleop 10 / Active 50	15%
Teleop 10 / Active 100	40%
Teleop 10 / Active 200	55%
Teleop 10 / Active 400	65%

TABLE V: Ablation on action formulation on Crate Stacking.

Action Formulation	Success Rate
Absolute Joint (q)	5%
Delta Joint (Δq)	40%

D. Scalability Analysis

To evaluate scalability, we fix the number of teleoperation demonstrations at 10 and progressively increase the number of Active demonstrations. As shown in Table IV, policy performance on the most challenging task (Crate Stacking) improves consistently as more Active data is incorporated.

With only 50 Active demonstrations, the policy achieves a limited 15% success rate, indicating insufficient coverage of the coordination space. Increasing the dataset to 100 and 200 Active episodes yields substantial gains, reaching 40% and 55% success, respectively. When scaled to 400 Active demonstrations, performance further improves to 65%, without exhibiting early saturation.

The monotonic improvement demonstrates that Active-collected data remains information-dense and policy-relevant as volume increases. Unlike teleoperation data, which is often constrained by perceptual indirection and accumulated control noise, Active demonstrations preserve consistent first-person visuomotor alignment and natural bimanual coordination. As a result, increasing the quantity of Active data directly translates into improved execution stability and task completion rates.

E. Ablation Study: Absolute vs. Delta-Joint Formulation

To isolate the impact of our shift-invariant action formulation, we replace the proposed Δq representation with direct absolute joint targets while keeping the training data fixed (Teleop 10 / Active 100). As shown in Table V, policy success rate on Crate Stacking collapses from 40% to 5% under absolute joint supervision.

The dramatic performance drop indicates that absolute joint representations are highly sensitive to static calibration offsets, structural compliance, and minor embodiment inconsistencies between demonstration and execution. Such systematic errors accumulate during long-horizon bimanual coordination, leading to unstable transport and misalignment during stacking.

In contrast, the Δq formulation inherently cancels constant offsets and focuses the policy on locally consistent motion increments. This shift-invariant representation yields substantially more stable trajectory reproduction and significantly

improves downstream imitation learning robustness.

F. Ablation Study: Impact of Subtask Annotations

TABLE VI: Ablation on Subtask Annotations. Both models are trained on the fixed Teleop 10 / Active 100 dataset and evaluated over 20 trials.

Architecture	Pick-and-Place	Blocks	Stacking
$\pi_{0.5}$	85%	60%	40%
$\pi_{0.5}^+$	85%	65%	50%

To isolate the contribution of our subtask annotation pipeline, we compare the standard $\pi_{0.5}$ baseline against our augmented $\pi_{0.5}^+$ architecture. Both policies are trained on the identical hybrid dataset (10 Teleoperation / 100 Active demonstrations) and evaluated over 20 independent trials per task. As detailed in Table VI, the baseline $\pi_{0.5}$ performs reliably on the short-horizon Pick-and-Place task (85%) but deteriorates as the execution horizon increases, dropping to 60% and 40% on the Blocks Collection and Crate Stacking tasks, respectively. Without explicit semantic guidance, the baseline struggles to maintain temporal consistency across extended multi-stage sequences.

In contrast, the autoregressive head of $\pi_{0.5}^+$ explicitly leverages language-conditioned subtask boundaries to enforce persistent stage awareness. While performance on the relatively brief Pick-and-Place task remains unchanged (85%), this temporal regularization proves critical for complex workflows. Consequently, $\pi_{0.5}^+$ yields a 5% absolute improvement on Blocks Collection (reaching 65%) and a substantial 10% absolute gain on the highly complex Crate Stacking task (reaching 50%). These results confirm that linguistically grounded subtask supervision effectively mitigates compounding errors in long-duration tasks without compromising short-horizon agility.

V. CONCLUSION

In this work, we introduced SuperSuit, a bimodal whole-body interface designed to scale data acquisition for mobile manipulation. By unifying active human demonstration and robot-in-the-loop teleoperation under a shared kinematic representation, SuperSuit effectively decouples data collection from hardware constraints while ensuring cross-modal consistency. The integration of drift-free locomotion retargeting and a delta-joint action formulation successfully mitigated execution discrepancies, ensuring high execution fidelity in long-horizon tasks. Furthermore, in-situ verbal narration streamlined the construction of multimodal datasets by enabling real-time language annotation. Experimental results validated that SuperSuit significantly enhances data throughput and enables policies to master complex bimanual coordination tasks. Future research will focus on incorporating haptic feedback for contact-rich interactions and extending the framework to heterogeneous embodiments for cross-platform data aggregation.

REFERENCES

- [1] T. Z. Zhao, V. Kumar, S. Levine, and C. Finn, "Learning fine-grained bimanual manipulation with low-cost hardware," *arXiv preprint arXiv:2304.13705*, 2023.
- [2] C. Chi, Z. Xu, S. Feng, E. Cousineau, Y. Du, B. Burchfiel, R. Tedrake, and S. Song, "Diffusion policy: Visuomotor policy learning via action diffusion," *The International Journal of Robotics Research*, vol. 44, no. 10-11, pp. 1684–1704, 2025.
- [3] K. Black, N. Brown, D. Driess, A. Esmail, M. Equi, C. Finn, N. Fusai, L. Groom, K. Hausman, B. Ichter, *et al.*, " π_0 : A vision-language-action flow model for general robot control," *arXiv preprint arXiv:2410.24164*, 2024.
- [4] K. Pertsch, K. Stachowicz, B. Ichter, D. Driess, S. Nair, Q. Vuong, O. Mees, C. Finn, and S. Levine, "Fast: Efficient action tokenization for vision-language-action models," *arXiv preprint arXiv:2501.09747*, 2025.
- [5] M. Shukor, D. Aubakirova, F. Capuano, P. Kooijmans, S. Palma, A. Zouitine, M. Aractingi, C. Pascal, M. Russi, A. Marafioti, *et al.*, "Smolvla: A vision-language-action model for affordable and efficient robotics," *arXiv preprint arXiv:2506.01844*, 2025.
- [6] M. J. Kim, K. Pertsch, S. Karamcheti, T. Xiao, A. Balakrishna, S. Nair, R. Rafailov, E. Foster, G. Lam, P. Sanketi, *et al.*, "Openvla: An open-source vision-language-action model," *arXiv preprint arXiv:2406.09246*, 2024.
- [7] M. J. Kim, C. Finn, and P. Liang, "Fine-tuning vision-language-action models: Optimizing speed and success," *arXiv preprint arXiv:2502.19645*, 2025.
- [8] J. Zhang, Y. Chen, Y. Xu, Z. Huang, Y. Zhou, Y.-J. Yuan, X. Cai, G. Huang, X. Quan, H. Xu, *et al.*, "4d-vla: Spatiotemporal vision-language-action pretraining with cross-scene calibration," *arXiv preprint arXiv:2506.22242*, 2025.
- [9] A. O'Neill, A. Rehman, A. Maddukuri, A. Gupta, A. Padalkar, A. Lee, A. Pooley, A. Gupta, A. Mandlekar, A. Jain, *et al.*, "Open x-embodiment: Robotic learning datasets and rt-x models: Open x-embodiment collaboration 0," in *2024 IEEE International Conference on Robotics and Automation (ICRA)*, pp. 6892–6903, IEEE, 2024.
- [10] S. Wu, X. Liu, S. Xie, P. Wang, X. Li, B. Yang, Z. Li, K. Zhu, H. Wu, Y. Liu, *et al.*, "Robocoin: An open-sourced bimanual robotic data collection for integrated manipulation," *arXiv preprint arXiv:2511.17441*, 2025.
- [11] A. Khazatsky, K. Pertsch, S. Nair, A. Balakrishna, S. Dasari, S. Karamcheti, S. Nasiriany, M. K. Srirama, L. Y. Chen, K. Ellis, *et al.*, "Droid: A large-scale in-the-wild robot manipulation dataset," *arXiv preprint arXiv:2403.12945*, 2024.
- [12] C. C. Kemp, A. Edsinger, H. M. Clever, and B. Matulevich, "The design of stretch: A compact, lightweight mobile manipulator for indoor human environments," in *2022 International Conference on Robotics and Automation (ICRA)*, pp. 3150–3157, IEEE, 2022.
- [13] Z. Fu, T. Z. Zhao, and C. Finn, "Mobile aloha: Learning bimanual mobile manipulation with low-cost whole-body teleoperation," *arXiv preprint arXiv:2401.02117*, 2024.
- [14] Y. Jiang, R. Zhang, J. Wong, C. Wang, Y. Ze, H. Yin, C. Gokmen, S. Song, J. Wu, and L. Fei-Fei, "Behavior robot suite: Streamlining real-world whole-body manipulation for everyday household activities," *arXiv preprint arXiv:2503.05652*, 2025.
- [15] Q. Ben, F. Jia, J. Zeng, J. Dong, D. Lin, and J. Pang, "Homie: Humanoid loco-manipulation with isomorphic exoskeleton cockpit," *arXiv preprint arXiv:2502.13013*, 2025.
- [16] R. Zhong, Y. Sun, J. Wen, J. Li, C. Cheng, W. Dai, Z. Zeng, H. Lu, Y. Zhu, and Y. Xu, "Humanoidexo: Scalable whole-body humanoid manipulation via wearable exoskeleton," *arXiv preprint arXiv:2510.03022*, 2025.
- [17] M. Shi, S. Peng, J. Chen, H. Jiang, Y. Li, D. Huang, P. Luo, H. Li, and L. Chen, "Egohumanoid: Unlocking in-the-wild loco-manipulation with robot-free egocentric demonstration," *arXiv preprint arXiv:2602.10106*, 2026.
- [18] W. Xu, Y. Cai, D. He, J. Lin, and F. Zhang, "Fast-lio2: Fast direct lidar-inertial odometry," *IEEE Transactions on Robotics*, vol. 38, no. 4, pp. 2053–2073, 2022.
- [19] C. Chi, Z. Xu, C. Pan, E. Cousineau, B. Burchfiel, S. Feng, R. Tedrake, and S. Song, "Universal manipulation interface: In-the-wild robot teaching without in-the-wild robots," *arXiv preprint arXiv:2402.10329*, 2024.
- [20] M. Xu, H. Zhang, Y. Hou, Z. Xu, L. Fan, M. Veloso, and S. Song, "Dexumi: Using human hand as the universal manipulation interface for dexterous manipulation," *arXiv preprint arXiv:2505.21864*, 2025.
- [21] R. Nai, B. Zheng, J. Zhao, H. Zhu, S. Dai, Z. Chen, Y. Hu, Y. Hu, T. Zhang, C. Wen, *et al.*, "Humanoid manipulation interface: Humanoid whole-body manipulation from robot-free demonstrations," *arXiv preprint arXiv:2602.06643*, 2026.
- [22] Z. Fu, Q. Zhao, Q. Wu, G. Wetzstein, and C. Finn, "Humanplus: Humanoid shadowing and imitation from humans," *arXiv preprint arXiv:2406.10454*, 2024.
- [23] X. Cheng, Y. Ji, J. Chen, R. Yang, G. Yang, and X. Wang, "Expressive whole-body control for humanoid robots," *arXiv preprint arXiv:2402.16796*, 2024.
- [24] T. He, Z. Luo, X. He, W. Xiao, C. Zhang, W. Zhang, K. Kitani, C. Liu, and G. Shi, "Omnih2o: Universal and dexterous human-to-humanoid whole-body teleoperation and learning," *arXiv preprint arXiv:2406.08858*, 2024.
- [25] Y. Li, Y. Lin, J. Cui, T. Liu, W. Liang, Y. Zhu, and S. Huang, "Clone: Closed-loop whole-body humanoid teleoperation for long-horizon tasks," in *9th Annual Conference on Robot Learning*, 2025.
- [26] J. Li, X. Cheng, T. Huang, S. Yang, R.-Z. Qiu, and X. Wang, "Amo: Adaptive motion optimization for hyper-dexterous humanoid whole-body control," *arXiv preprint arXiv:2505.03738*, 2025.
- [27] Y. Ze, Z. Chen, J. P. Araújo, Z.-a. Cao, X. B. Peng, J. Wu, and C. K. Liu, "Twist: Teleoperated whole-body imitation system," *arXiv preprint arXiv:2505.02833*, 2025.
- [28] Y. Ze, S. Zhao, W. Wang, A. Kanazawa, R. Duan, P. Abbeel, G. Shi, J. Wu, and C. K. Liu, "Twist2: Scalable, portable, and holistic humanoid data collection system," *arXiv preprint arXiv:2511.02832*, 2025.
- [29] K. Liu, C. Guan, Z. Jia, Z. Wu, X. Liu, T. Wang, S. Liang, P. Chen, P. Zhang, H. Song, *et al.*, "Fastumi: A scalable and hardware-independent universal manipulation interface with dataset," *arXiv preprint arXiv:2409.19499*, 2024.
- [30] H. Choi, Y. Hou, C. Pan, S. Hong, A. Patel, X. Xu, M. R. Cutkosky, and S. Song, "In-the-wild compliant manipulation with umi-ft," *arXiv preprint arXiv:2601.09988*, 2026.
- [31] S. Liu, B. Li, K. Ma, L. Wu, H. Tan, X. Ouyang, H. Su, and J. Zhu, "Rdt2: Exploring the scaling limit of umi data towards zero-shot cross-embodiment generalization," *arXiv preprint arXiv:2602.03310*, 2026.
- [32] F. Lin, R. Nai, Y. Hu, J. You, J. Zhao, and Y. Gao, "Onetwovla: A unified vision-language-action model with adaptive reasoning," *arXiv preprint arXiv:2505.11917*, 2025.
- [33] N. M. M. Shafiqullah, A. Rai, H. Etukuru, Y. Liu, I. Misra, S. Chintala, and L. Pinto, "On bringing robots home," *arXiv preprint arXiv:2311.16098*, 2023.
- [34] H. Ha, Y. Gao, Z. Fu, J. Tan, and S. Song, "Umi on legs: Making manipulation policies mobile with manipulation-centric whole-body controllers," *arXiv preprint arXiv:2407.10353*, 2024.
- [35] T. Portela, A. Cramariuc, M. Mittal, and M. Hutter, "Whole-body end-effector pose tracking," in *2025 IEEE International Conference on Robotics and Automation (ICRA)*, pp. 11205–11211, IEEE, 2025.
- [36] H. Kim, Y. Ohmura, A. Nagakubo, and Y. Kuniyoshi, "Training robots without robots: Deep imitation learning for master-to-robot policy transfer," *IEEE Robotics and Automation Letters*, vol. 8, no. 5, pp. 2906–2913, 2023.
- [37] H. Fang, H.-S. Fang, Y. Wang, J. Ren, J. Chen, R. Zhang, W. Wang, and C. Lu, "Airexo: Low-cost exoskeletons for learning whole-arm manipulation in the wild," in *2024 IEEE International Conference on Robotics and Automation (ICRA)*, pp. 15031–15038, IEEE, 2024.
- [38] H. Fang, C. Wang, Y. Wang, J. Chen, S. Xia, J. Lv, Z. He, X. Yi, Y. Guo, X. Zhan, *et al.*, "Airexo-2: Scaling up generalizable robotic imitation learning with low-cost exoskeletons," *arXiv preprint arXiv:2503.03081*, 2025.
- [39] Z. Gao, S. Zhang, I. McLoughlin, and Z. Yan, "Paraformer: Fast and accurate parallel transformer for non-autoregressive end-to-end speech recognition," *arXiv preprint arXiv:2206.08317*, 2022.
- [40] A. Yang, A. Li, B. Yang, B. Zhang, B. Hui, B. Zheng, B. Yu, C. Gao, C. Huang, C. Lv, *et al.*, "Qwen3 technical report," *arXiv preprint arXiv:2505.09388*, 2025.
- [41] K. Black, N. Brown, J. Darphinian, K. Dhabalia, D. Driess, A. Esmail, M. R. Equi, C. Finn, N. Fusai, M. Y. Galliker, *et al.*, " $\pi_{0.5}$: A vision-language-action model with open-world generalization," in *9th Annual Conference on Robot Learning*, 2025.